J Electroceram (2008) 20:119–126
DOI 10.1007/s10832-007-9376-z

Studies of structural, dielectric and impedance properties of $Bi_9Fe_5Ti_3O_{27}$ ceramics

S. K. Patri · R. N. P. Choudhary · B. K. Samantaray

Received: 21 May 2007 / Accepted: 22 November 2007 / Published online: 21 December 2007
© Springer Science + Business Media, LLC 2007

Abstract $Bi_9Fe_5Ti_3O_{27}$ is an eight-layered material belonging to the family of bismuth layered structured ferroelectromagnets. The polycrystalline sample of this compound was prepared by a standard solid-state reaction technique. The formation of the compound in an orthorhombic crystal structure was confirmed by an X-ray diffraction (XRD) technique (lattice parameters: a=5.5045 [27] Å, b=5.6104[27] Å, c=76.3727[27] Å). Detailed studies of surface morphology of the compound using scanning electron microscopy (SEM) exhibit that the compound has domains of plate shaped grains. Studies of dielectric and electric properties in a wide temperature range (30–500 °C) at different frequencies (100 Hz–1 MHz) exhibit an anomaly at 291±2 °C, which is related to ferroelectric to paraelectric phase transition as suggested by hysteresis loop at room temperature. The values and nature of temperature variation of dc conductivity exhibit the NTCR behavior of the compound.

Keywords X-ray diffraction · Surface morphology · Dielectric properties

1 Introduction

Bismuth layered perovskite compounds of a general formula $A_{m-1}Bi_2B_mO_{3m+3}$ having Aurivillius phases [1] are built with layers of $(Bi_2O_2)^{2+}$ and $(A_{m-1}B_mO_{3m+1})^{2-}$ slabs, where A and B are combination of ions for dodecahedrally and octahedrally coordinated interstices respectively and m (integer) is the number of perovskite layers [2, 3]. These compounds can be derived from the $Bi_4Ti_3O_{12}/BiFeO_3$ system, which have semiconducting, ferroelectric and ferromagnetic properties. These bismuth layered compounds were synthesised by solid state reaction technique and characterized by X-ray diffraction (XRD) by Morosov et al. [4]. On increasing the number of perovskite layers (m), the microstructure and physical properties of the materials can be changed significantly. Further, some of the Fe containing compounds of this family show simultaneous ferroelectric and ferromagnetic properties, and hence exhibit magnetoelectric (ME) effect under the influence of an external magnetic/electric field [5]. Because of the existence of ME effect, anisotropic electronic, dielectric, optical and ionic properties, these materials have a wide range of multifunctional applications in spintronics, information storage devices such as multi-state nonvolatile memories, sensors, phase shifters, amplitude modulators and electro-optic devices etc. [6]. Recently, ME effect has been reported in many distorted layered perovskites and in $BiFeO_3$ [7], $YMnO_3$ [8], $BiMnO_3$ [9] etc. The ME effect in many compounds of this family were reported much earlier by Smolenskii et al. [10] and Subbarao [11] for $1 \leq m \leq 8$. On the basis of electro-microscopic study, it has been shown that ME effect is also possible in a mixture of compounds having m=4 and m=5 [12, 13]. It has been reported earlier that the eight-layered compound ($Bi_9Fe_5Ti_3O_{27}$) has an orthorhombic crystal structure at room temperature [14]. Investigations of magnetic properties showed that this compound is antiferromagnetic (T_N=130 °C) with a weak ferromagnetism. The compound $Bi_9Fe_5Ti_3O_{27}$ first behaves like a superparamagnet, and transformed to an antiferromagnetic state around 400 K [15, 16]. In recent years, there has been a growing interest in magnetoelectric materials because of their potential applications for both magnetic

S. K. Patri · R. N. P. Choudhary (✉) · B. K. Samantaray
Department of Physics and Meteorology, IIT,
Kharagpur 721 302, India
e-mail: crnpfl@phy.iitkgp.ernet.in

and ferroelectric devices. Also, the ability to couple the charge and spin order parameters of these materials provides an additional degree of freedom for designing multifunctional devices. Besides their potential applications, study of the fundamental physics of magnetoelectric materials is also fascinating. Detailed literature survey on structure, microstructure and electrical properties of the titled compound show that these said properties have not been reported so far. Therefore, this paper mainly reports the structural and electrical properties of $Bi_9Fe_5Ti_3O_{27}$ ceramic.

2 Experimental

The polycrystalline sample of $Bi_9Fe_5Ti_3O_{27}$ (BFTO) was prepared using a high-temperature solid-state reaction technique. Stoichiometric amount of AR grade (≥99.9% purity) precursors Bi_2O_3, Fe_2O_3, TiO_2 were mixed thoroughly first in an agate mortar and pestle for 2 h and then by mechanical grinding in wet (alcohol) atmosphere to achieve homogeneous mixture of the constituents. The sample was calcined twice at 950°C for 8 h in air atmosphere. The calcined powder was uniaxially cold pressed into cylindrical pellets (0.97 cm diameter and 0.192 cm thickness) with polyvinyl alcohol (PVA) as a binder. These pellets were sintered at an optimized temperature and time (1000°C for 8 h). The sintered pellets were electroded with conductive silver paint followed by slow drying. The formation of the single phase compound was confirmed by XRD studies. The XRD pattern of the material was recorded at room temperature using an X-ray powder diffractometer (Rigaku, Miniflex) in a wide range of Bragg angles ($20°\leq 2\theta \leq 80°$) with CuK_α radiation (1.5405 Å) at a scan speed of 4°/min. The X-ray diffraction data was used to evaluate the density (ρ_{th}) using the formula; $\rho_{th} = \frac{(\sum A/N)}{V} n$; where ρ_{th} is the theoretical density (g/cm^3), $\sum A$ is the sum of the atomic weights of all the atoms in the unit cell, N is the Avogadro's number, V is the volume of the unit cell (cm^3) and n is the number of atoms per unit cell of the crystal structure. The density so evaluated was compared with the measured density of the sample and the percent of sample porosity was calculated using the following relations:

$$\rho_{exp} = \frac{\text{mass of the pellet}}{\text{volume of the pellet}},$$

$$\text{and \% porosity} = \frac{\left(\rho_{th} - \rho_{exp}\right)}{\rho_{th}} \times 100$$

Scanning electron micrographs of the material were recorded with a high-resolution scanning electron microscope (SEM: JOEL-JSM, model: 5800F) to study the surface morphology/microstructure of the pellet sample. The pellet was gold coated prior to being scanned under high-resolution field emission gun of SEM. Dielectric and impedance parameters are measured using a computer-controlled frequency response analyzer (HIOKI LCR HI Tester, Model: 3532) as a function of temperature over a wide range of frequencies (100 Hz–1 MHz) after drying the silver coated sample at 150 °C for 2 h. The hysteresis loop of the poled sample (13 kV/cm for 48 h) was obtained using workstation of loop tracer, (M/S Radiant Technology Inc, USA). Because of the high leakage current of Fe containing compound, it was difficult to pole this sample properly at high electric field and elevated temperature.

3 Results and discussion

3.1 Structural analysis

The XRD pattern of the sintered sample is shown in Fig. 1. All the peaks are indexed using standard computer software "POWDMULT" [17]. Detailed structural analysis in different crystal structure and cell constants exhibit that the sample has an orthorhombic structure with lattice parameters: a=5.5045(27) Å, b=5.6104(27) Å, c=76.3727(27) Å (estimated standard deviation in parenthesis), which is in well agreement with the orthogonal structure given in ICDD card number 21-0100. The microdensity (loosely speaking the theoretical density) of the compound is calculated as ~5 g/cm^3 and the corresponding bulk (experimental density) of the compound is ~4.6 g/cm^3. Thus, the experimental density of the sample was found as 92% of the theoretical density. The crystallite size of the powder sample was roughly estimated from the broadening

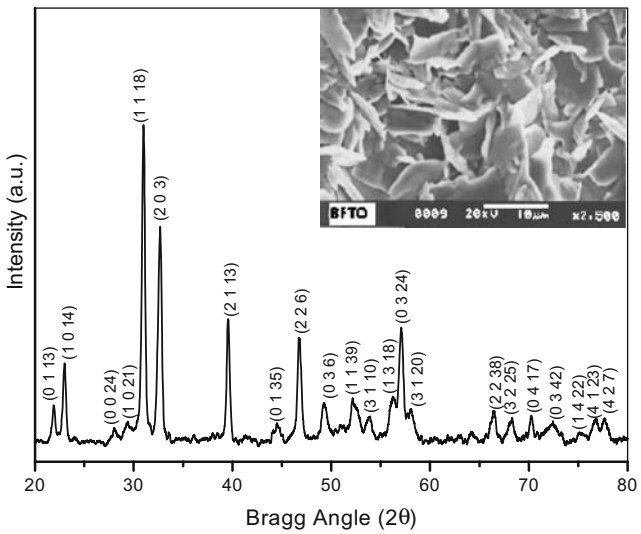

Fig. 1 Room temperature XRD pattern of $Bi_9Fe_5Ti_3O_{27}$, SEM of the compound is shown *inset* of this figure

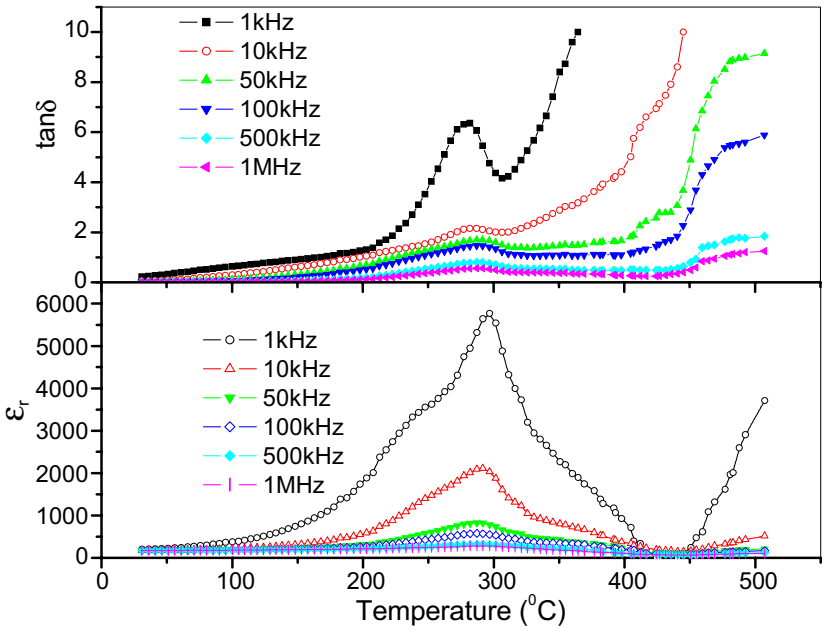

Fig. 2 Variation of dielectric constant (ε) and dielectric loss (tanδ) of BFTO with temperature at different frequencies

of reflection peaks using Scherrer's equation, $P = \frac{0.89\lambda}{\beta_{1/2}\cos\theta}$ [18, 19], where $\lambda = 1.5405$ Å and $\beta_{1/2}$=half peak width of reflections. The average crystallite size was found to be 15 nm (ignoring broadening due to strain and other effects).

The SEM micrograph of the sample is shown in the inset of Fig. 1. The platelet-like grains were observed which is very much similar to that of other compounds of this family [5, 20]. The grains are distributed homogeneously throughout the surface of the sample. The average grain size was found to be 9 μm.

3.2 Dielectric study

Figure 2 shows the variation of relative dielectric constant (ε_r) and loss tangent (tanδ) with temperature of BFTO at different frequencies. The values of ε_r for the compound increase gradually with rise in temperature up to a certain temperature (which is usually referred as transition temperature [T_c]), and thereafter, it decreases. The dielectric anomaly suggests that there is a probability of phase transition of the ferroelectric to paraelectric type at 291±2 °C. The values of dielectric constant and loss tangent at room temperature are given in Table 1. We also observed that the values of dielectric constant decreases with increase in frequency. It indicates the presence of all types of polarizations (i.e., ionic, dipole, atomic, electronic etc.) in the material at lower frequencies.

The *P–E* loop of $Bi_9Fe_5Ti_3O_{27}$ is shown in Fig. 3, in which a small expected polarization of $2P_r$=0.038 μC/cm^2 was found. Though remanent polarization of the sample is very small, it confirms the ferroelectric property of the sample.

Table 1 Values of relative dielectric constant and loss tangent of $Bi_9Fe_5Ti_3O_{27}$ at room temperature.

Frequency in kHz	ε_r	tanδ
1	200	0.2339
10	177	0.0527
50	174	0.0267
100	173	0.0266
500	170	0.0192
1000	169	0.0146

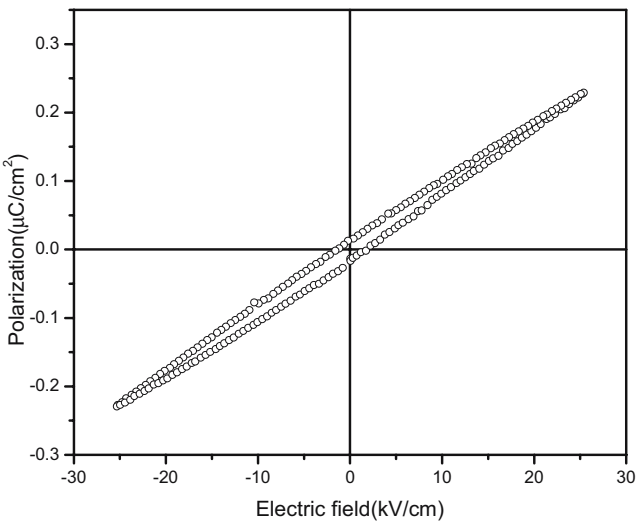

Fig. 3 *P–E* loop of $Bi_9Fe_5Ti_3O_{27}$ at room temperature

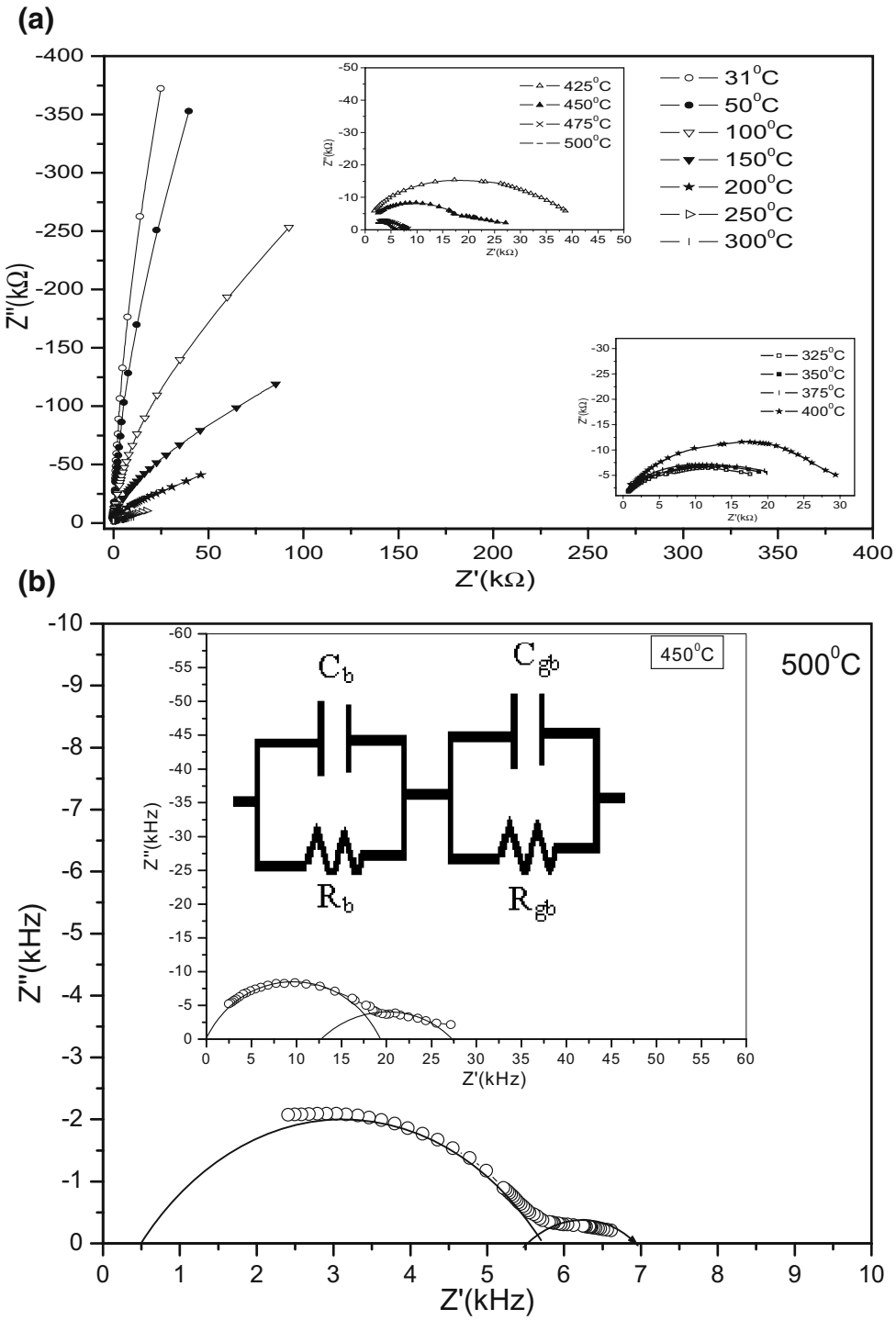

Fig. 4 (**a**) Nyquist plots of BFTO at different temperature. (**b**) Nyquist plots of BFTO with equivalent circuit (*inset*)

3.3 Impedance analysis

The electrical behavior of the system was studied over a wide range of frequency and temperature using a complex impedance spectroscopy technique (CIS). This technique enables us to separate the real and imaginary components of the complex impedance parameters, and hence provides information of the structure–property relationship of the sample. A polycrystalline material usually has grain and grain boundary properties with different time constants at high temperature leading to two successive semicircles. It can conventionally be displayed in a complex plane plot (Nyquist diagram) in terms of the following formalism:

$$\text{Complex impedance, } Z^*(\omega) = Z' - jZ'' \quad (1)$$

Complex permittivity, $\varepsilon^*(\omega) = \varepsilon' - j\varepsilon''$ (2)

Complex modulus, $M^*(\omega) = 1/\varepsilon(\omega) = M' + M''$ (3)

where $Z' = |Z| \cos\theta$ and $Z'' = |Z| \sin\theta$

Figure 4(a) shows a set of Nyquist plots (Z' vs Z'') over a wide range of frequency (100 Hz–1 MHz) at different temperature. The effect of temperature on impedance parameter of the material becomes clearly visible with rise in temperature. The straight lines with large slopes at lower temperatures indicate the insulating behavior of the material. However, on increasing temperature, the slope of the lines decreases, and hence they bend towards Z'-axis by which semicircle could be formed. The intercept of the semicircle on the real axis is the bulk resistance (R_b) of the sample. At much higher temperatures (≥450 °C), it was possible to trace two semicircles (Fig. 4(b)). The appearance of two semicircles suggests the presence of both bulk as well as grain boundary effects in the polycrystalline sample. Each semicircle is a representative of an *RC* circuit that corresponds to individual component of the material (Fig. 4(b) [*inset*]).

Figure 5(a) exhibits the variation of real part of impedance (Z') with frequency at different temperature. The decrease in the magnitude of Z' with increase in both

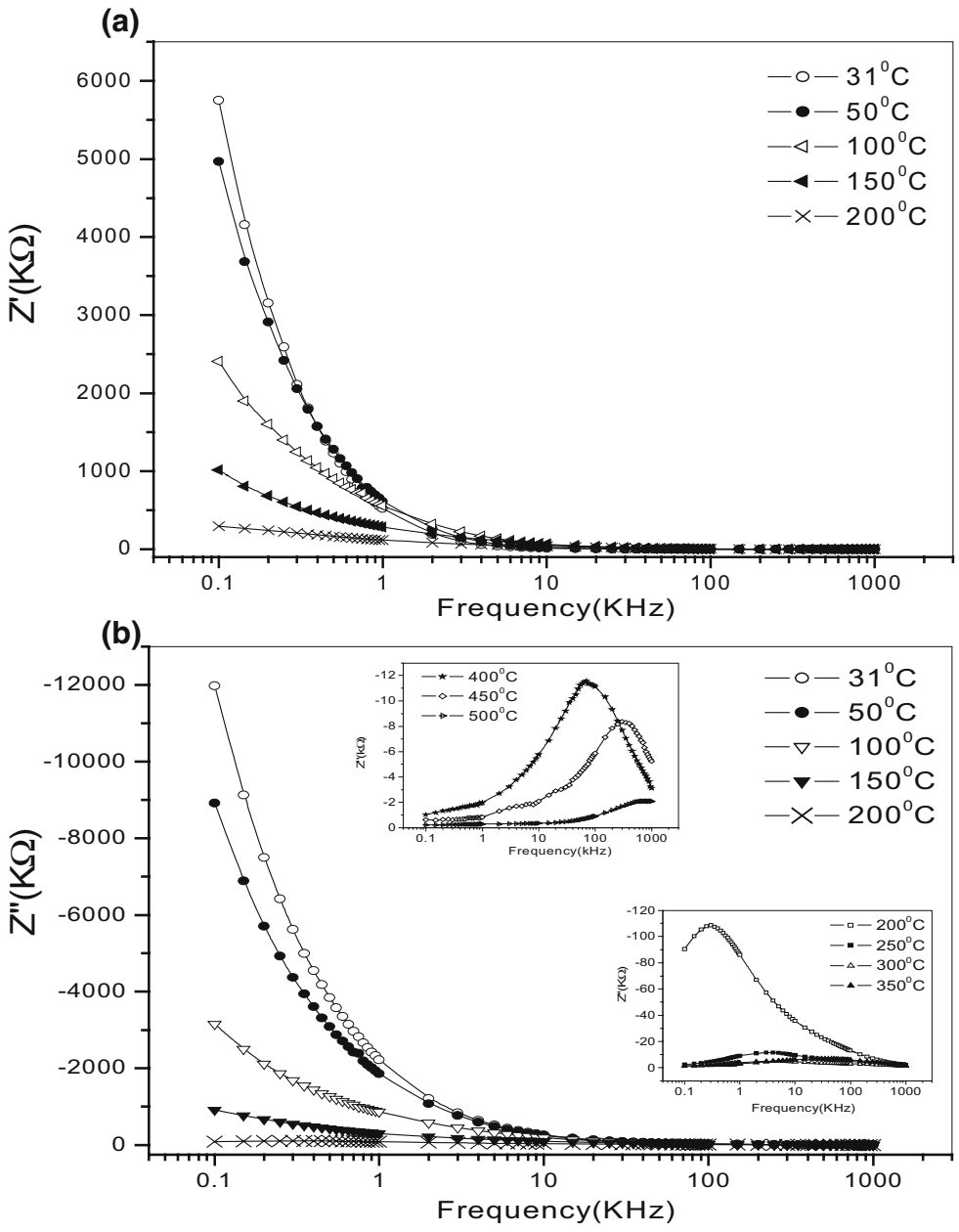

Fig. 5 Variation of (**a**) real part of impedance (Z') and (**b**) imaginary part of impedance (Z'') of BFTO as a function of frequency

frequency as well as temperature indicates the increase in ac conductivity. The values of Z' merge at higher frequencies (≥10 kHz) which indicates the release of space charges. Figure 5(b) represents the impedance loss spectrum (i.e., variation of imaginary part of impedance [Z''] with frequency). The nature of the pattern is characterized by (1) a decrease in the height of the peaks with rise in temperature, (2) significant broadening of the peaks with rise in temperature, and (3) marked asymmetry in the peak pattern. The curves show that the value of Z'' reaches maximum value of $Z''_{\max}$ for the temperatures ≥200 °C. The relaxation time (τ) was calculated from the frequency maxima ($f_{\max}$) at $Z''_{\max}$. At the peak, the relaxation is defined by the condition:

$$\omega_m \tau_m = 2\pi f_{\max} = 1 \tag{4}$$

where τ_m is the relaxation time at $f_{\max}$ and $f_{\max}$ is the relaxation frequency. It is independent of the sample geometrical factors and depends basically on the intrinsic properties (i.e., microstructure) of the material only. A typical variation of τ as a function of temperature is shown in Fig. 6. The pattern shows a steady increase in the relaxation time with temperature. This result suggests the presence of temperature-dependent electrical relaxation phenomenon in the material possibly due to the migration of immobile species/defects. The typical variation appears to be of Arrhenius type:

$$\tau = \tau_0 \exp(-E_a/k_b T) \tag{5}$$

where τ_0=pre-exponential factor, E_a=activation energy E_a=activation energy and k_b=Boltzmann constant. The calculated activation energy of the sample is 0.87 eV in the high temperature region (200–500 °C).

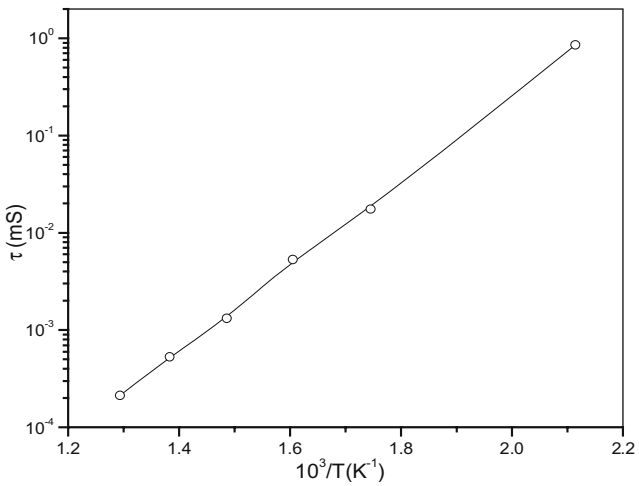

Fig. 6 Variation of relaxation time (τ) as a function of temperature

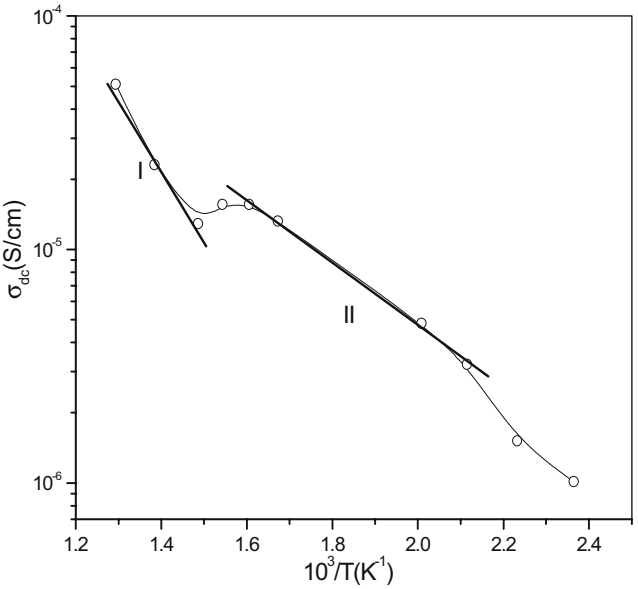

Fig. 7 Variation of dc conductivity (bulk) of BFTO as a function of temperature

3.4 Conductivity analysis

The electrical conductivity (dc and ac) of the material has been investigated at different temperatures over a wide range of frequency.

3.4.1 dc conductivity

The dc electrical conduction (σ_{dc}) is a thermally activated process. Figure 7 shows the variation of dc conductivity (σ_{dc}) as a function of temperature. Here the conductivity increases with a rise in temperature. It can be explained by using the relation:

$$\sigma_{dc} = \sigma_0 \exp(-E_a/k_b T) \tag{6}$$

where σ_0=pre-exponential factor and E_a is activation energy and k=Boltzmann constant. The activation energy, calculated from the slope of the log σ_{dc} versus $1/T$ plot in different temperature regions I and II was found to be 0.59, 0.26 eV, respectively. Oxygen vacancies and space charge may be responsible for the change in the activation energy as a function of temperature. The loss of bismuth ions during high temperature treatment in layered perovskite would lead to oxygen vacancies.

3.4.2 ac conductivity

The temperature dependence of ac conductivity at different frequencies can be calculated from the dielectric data using the relation $\sigma_{ac}=\omega\varepsilon_0\varepsilon_r \tan\delta$ (7), where ε_r= relative dielectric constant and ε_0=dielectric constant in free space.

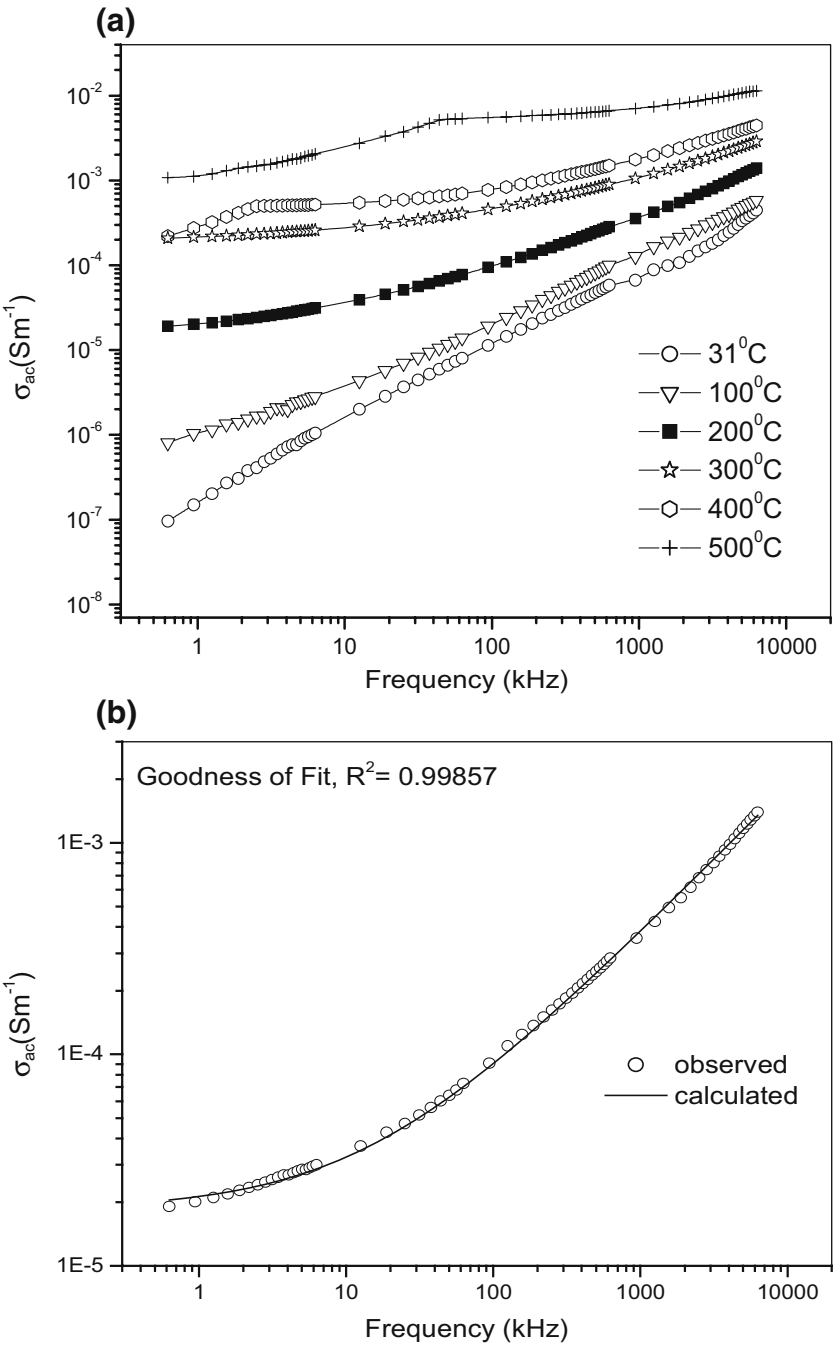

Fig. 8 (**a**) Variation of ac conductivity of BFTO with frequency at different temperatures. (**b**) Non-linear fitting of ac conductivity obeying Jonscher's universal power law

The frequency dependence of ac conductivity, $\sigma(\omega)$, at various temperature is shown in Fig. 8(a). At low temperatures the conductivity increases with rise in frequency, which is a characteristic of ω^n (n=exponential). At high temperatures and low frequencies conductivity shows a flat response while it has a ω^n dependence at high frequencies. The phenomenon of the conductivity dispersion in solids is generally analyzed using Jonscher's power law; $\sigma(\omega) = \sigma_0 + A\omega^n$, where σ_0 is the dc conductivity at a particular temperature, A is a temperature dependent constant and n is the temperature dependent power law exponent in the range of $0 \leq n \leq 1$. The exponent n represents the degree of interaction between mobile ions with the lattice around them, and the pre exponential factor. A determines the strength of polarizability. The material obeys the universal power law, and is confirmed by a typical fit of the above equation to the experimental data at 200 °C (Fig. 8(b)). The value of n was found to be ~0.70. According to

Jonscher, the origin of frequency dependence of conductivity lies in the relaxation phenomenon arising due to mobile charge carriers. The low frequency dispersion has been attributed to the ac conductivity whereas the frequency independent plateau region of the conductivity pattern corresponds to dc conductivity of the material. The temperature, at which grain resistance dominates over grain boundary resistance, is marked by a change in slope of ac conductivity with frequency. The frequency at which the change of slope takes place is known as the hopping frequency. It corresponds to polaron hopping of charged species. The hopping frequency shifts to higher frequency side on increasing temperature. The charged species that have been accumulated at the grain boundaries have sufficient energy to jump over the barrier on increasing temperature.

4 Conclusions

The $Bi_9Fe_5Ti_3O_{27}$ ceramic was prepared by a high-temperature solid-state reaction technique. X-ray structural study reveals an orthorhombic crystal structure of this material. The surface morphology of the compound is studied through SEM, which shows the uniform distribution of grains through out the sample. The electrical parameters such as the real and imaginary parts of impedance and ac/dc conductivity as a function of both frequency and temperature have been studied through complex impedance spectroscopy. Niquist plots show the presence of bulk and grain boundary effects in this system. The nature of variation of (ac/dc) conductivity with temperature exhibits the NTCR behavior of the sample like that of a semiconductor.

References

1. B. Aurivillius, Arki. Kemi. **1**, 499 (1949)
2. B. Aurivillius, Arki. Kemi. **1**, 463 (1949)
3. I.H. Ismailzade, V.I. Nesternenko, F.A. Mirishli, P.G. Rustamov, Sov. Phys. Crystallogr. **12**, 400 (1967)
4. M.I. Morosov, V.V. Gusarov, Russ. J. Inorg. Mater. **38**, 723 (2002)
5. A. Srinivas, M. Mahesh Kumar, S.V. Suryanarana, T. Bhimasankaram, Mater. Res. Bull. **34**, 989 (1999)
6. M. Miyayama, J. Ceram. Soc. Jpn. **114**, 583 (2006)
7. J. Wang, J.B. Neaton, H. Zheng, V. Nagarajan, S.B. Ogale, B. Liu, D. Viehland, V. Vaithyanathan, D.G. Schlom, U.V. Waghmare, N. A. Spaldin, K.M. Rabe, M. Wuttig, R. Ramesh, Science **299**, 1719 (2003)
8. B.B. Van Aken, T.T.N. Palstra, A. Filippetti, N.A. Spaldin, Nature **3**, 164 (2004)
9. T. kimura, S. Kawamoto, I. Yamada, M. Azuma, M. Takano, T. Tokura, Phys. Rev. B **67**, 180401 (2003)
10. G.A. Smolenskii, V.A. Isupov, A.I. Agranovskaya, Fiz. Tverd. Tela (Leningr) **3**, 895 (1961)
11. E.C. Subbarao, J. Am. Ceram. Soc. **45**, 166 (1962)
12. I.H. Ismailzade, F.A. Mirishli, Izv. Akad. Nauk. SSR Ser. Fiz. **33**, 1138 (1969)
13. J.L. Hutchinson, J.S. Anderson, C.N.R. Rao, Proc. R. Soc. Lond. A **355**, 301 (1977)
14. I.H. Ismailzade, R.G. Yakupov, T.A. Melik-Shanazarova, Phys. Stat. Sol. A **6**, K85 (1971)
15. G.D. Sultanov, N.G. Gueseinov, I.H. Ismailzade, R.M. Mirzababaev, L.A. Aliev, Sov. Phys. Solid State **7**, 1271 (1975)
16. M. Krzhizhanovskaya, S. Filatov, V. Gusarov, P. Paufler, R. Bubnova, M. Morozov, D.C. Meyer, Z. Anorg. Allg. Chem. **631**, 1603 (2005)
17. POWDMULT: An interactive powder diffraction data interpretations and indexing Program Version 2.1, E. WU School of Physical Sciences, Flinder University of South Australia Bradford Park, SA 5042, Australia
18. H.P. Klug, L.B. Alexander, X-ray Diffraction Procedures (Wiley, New York (1974)
19. B.D. Cullity, Elements of X-Ray Diffraction (Addison-Wesley, Philipines (1978)
20. I. Pribosic, D. Makovac, M. Drofenik, J. Eur. Ceram. Soc. **21**, 1327 (2001)